Earth and Planetary Science Letters 293 (2010) 54–62

Contents lists available at ScienceDirect

Earth and Planetary Science Letters

journal homepage: www.elsevier.com/locate/epsl

Large angle reflection from a dipping structure recorded as a PKIKP precursor: Evidence for a low velocity zone at the core–mantle boundary beneath the Gulf of Mexico

Elizabeth Vanacore *[,1], Fenglin Niu, Yanlu Ma [2]

Department of Earth Science, MS-126, Rice University, 6100 Main St., Houston, TX 77005, USA

ARTICLE INFO

Article history:
Received 29 April 2009
Received in revised form 16 November 2009
Accepted 14 February 2010
Available online 19 March 2010

Editor: L. Stixrude

Keywords:
PKIKP precursor
dipping reflector
ultralow-velocity zone
Farallon slab
Gulf of Mexico

ABSTRACT

We observed a clear phase-like arrival prior to the PKIKP wave at a broadband seismic array in eastern Tibet from an intermediate depth earthquake occurring in Guatemala. The measured incident angle and back azimuth of this phase indicate that it originates from scattering near the core–mantle boundary (CMB) of the source side. This phase, however, was not observed from another earthquake that is only 60 km away, suggesting that scattering depends strongly on the angles of the incident waves. Ray tracing and diffraction migration indicates that the precursor is a large-angle reflection from a dipping structure in the lowermost mantle east of Mexico. The seismic reflector dips northward by ~52° and is centered at ~93.31°W and 23.89°N with an east–west extension of ~100 km. A decrease of P-wave velocity by a few to 10% is required to explain the amplitude and polarity of the phase. It is unlikely to explain the large P-wave velocity contrast and the large dipping feature with the post-perovskite phase transition. The reflector is located in a region where the lowermost mantle is marked by a high velocity anomaly related to the subducted Farallon slab. Previous numerical modeling suggested that a substantial amount of hot mantle could be trapped beneath a slab over long periods of time, leading to the formation of a mega-plume. Thus, the observed sharp dipping boundary here might correspond to the edge of a low velocity zone below the subducted Farallon slab. Mixed results on the presence of an ultra low velocity zone in the region have been reported by previous seismic studies. We speculated that the low velocity zone below the cold slab was developed as a consequence of long-term heating from core.

1. Introduction

The lowermost several hundreds kilometers of the Earth's mantle (the D″ layer) above the core–mantle boundary (CMB) is known to be extremely heterogeneous in terms of seismic structure (see Garnero, 2004; Lay and Garnero, 2004, for reviews). Among various types of seismic structures, the ultralow-velocity zones and small-scale seismic scatterers (Cleary and Haddon, 1972; Doornbos and Husebye, 1972; Garnero et al. 1993; Hedlin et al., 1997; Wen and Helmberger, 1998; Vidale and Hedlin 1998; Hedlin and Shearer, 2000; Niu and Wen 2001; Cao and Romanowicz, 2007; Miller and Niu, 2008) are very unique and their origins are still debated. Intermittent zones with extreme P- and S-wave velocity decreases of up to 10% and 30%, respectively, have been recently imaged within the lowermost 5 to 40 km of the Earth's mantle (Thorne and Garnero, 2004; Rost et al., 2005). Such thin patches were often interpreted as resulting from partial melt that has accumulated at the CMB given that the Vs to Vp ratio of the velocity perturbation is on the order of 3 to 1 (Williams and Garnero, 1996). Mao et al. (2006), on the other hand, found that iron-rich post perovskite (ppv) can match the observed seismic characteristics of ultra low velocity zones (ULVZs). They further suggested that a thin Fe-rich ppv silicate layer could form through chemical reaction between the silicate mantle and the iron core.

Because of the special ray geometry arising from the sharp velocity drop at the CMB, scattered energy from small-scale inhomogeneities in the lowermost mantle can arrive before the main PKIKP arrival (Cleary and Haddon, 1972). These early arrivals can be clearly observed in short-period seismograms, providing a unique opportunity to study small-scale seismic structures in the deep mantle that are not resolvable with traveltime tomography. Global observations indicated that PKIKP precursors form a continuous wave chain that are best explained by a random scattering field uniformly distributed in the bottom 200 km (Haddon and Cleary, 1974), and perhaps in a broader depth range (Hedlin et al., 1997) of the lower mantle. The scatterers are found to be smaller than 10 km with a ~1% velocity difference from the ambient mantle (Hedlin et al., 1997). These scatterers could be heterogeneities in seismic velocity and density, CMB topography, or both. The nature and origin of these small-scale heterogeneities, however, remain elusive, although there are many

* Corresponding author.
E-mail address: elizabeth.vanacore@anu.edu.au (E. Vanacore).
[1] Present address: The Australian National University, Research School of Earth Sciences, Bldg 61 Mills Rd, Canberra, Australia.
[2] Present address: Helmholtz Center Potsdam, GFZ German Research Centre for Geosciences, Telegrafenberg 14473, Potsdam, Germany.

0012-821X/$ – see front matter © 2010 Elsevier B.V. All rights reserved.
doi:10.1016/j.epsl.2010.02.018

speculations that they might be associated with subducted slabs (Helffrich and Wood, 2001). Meanwhile, anomalous PKIKP precursors with either large amplitude or distinct waveforms are also observed in different tectonic regions (e.g., Vidale and Hedlin, 1998; Wen and Helmberger, 1998; Thomas et al., 1999; Wen, 2000; Niu and Wen, 2001; Cao and Romanowicz, 2007). They were interpreted as stemming from strong inhomogeneities that might be related to partial melt. Regardless whether weak or strong heterogeneities are invoked, PKIKP precursors are generally attributed to scattering by small-scale volumetric anomalies (scatterers) rather than reflecting from areal anomalies (reflectors).

In this study, we investigated some unique features of PKIKP precursors recorded by a broadband array in Tibet from two intermediate depth earthquakes. Our analysis indicated that the observed precursors are better explained by a reflection at a high-to-low velocity boundary rather than scattering from randomly distributed scatterers (Fig. 1). We interpreted the boundary as the edge of a low velocity zone lying under the subducted Farallon slab beneath the Gulf of Mexico that was developed by long-term heating from the core.

2. PKP precursors observed at the Namche Barwa array

We examined data from intermediate depth earthquakes occurring in Central America recorded at the Namche Barwa array (Meltzer et al., 2003) in Tibet to search for PKP precursory arrivals in the epicentral distances between 130° and 140° (Fig. 2). Broadband seismograms with high signal-to-noise ratio (SNR) from two intermediate depth earthquakes were selected for analysis (Table 1). Recordings of the event 08/25/2003 exhibited a clear phase before the PKP arrival (Fig. 3a). The observed precursor is a highly coherent and well-aligned signal. The precursor has amplitude approximately 20% as large as the main PKIKP arrival. This is very different from general observations of PKP precursors, which are featured by a continuous wave packet lasting for tens of seconds. Here we filtered the broadband seismograms with a filter that mimics the instrument response of a WWSSN (World Wide Standard Seismic Network) short-period sensor. On the other hand, this phase-like signal is, however, not observed in the array recordings of the event 05/03/2004 (Fig. 3b), which is only 60 km away from the event 08/25/2003 (Fig. 2).

Fig. 3c and d show the scattering area of the two earthquakes at the CMB in the source side that would generate precursory arrivals to the main PKIKP phase. The earthquakes share almost the same scattering fields (blue area in Fig. 3c and d). This is also true for the scattering area in the receiver side. If the scatterers in the two regions are isotropic in terms of radiating seismic waves, then these waves should be recorded as PKIKP precursors by both events. We noticed that the data quality of the 2004 event is significantly lower than the 2003 event. We calculated the signal-to-noise ratio (SNR) of the individual records of this event. Some of the stations showed a SNR of ≥ 10, so the precursor recorded by the 2004 event should be observable in the recordings of these stations. In fact, we computed the vespagram of the 2004 event and could not find any coherent arrivals in the time window before the PKIKP phase. This observation suggests that that interacting with the seismic anomaly is highly anisotropic. Just like a seismic reflector, this anomaly can scatter incoming energy only to a preferred direction.

We also noticed that the onsets of the observed precursor phase in the 2003 event are a few seconds later than the first precursory arrival predicted by models with scatterers being randomly distributed at the base of the mantle. All these suggest that the scatterer generating the observed early arrival is likely to be uneven in distribution and irregular in shape, very different from what Haddon and Cleary (1974) proposed. To better understand the origin of the scatterer, we investigated its location and geometry with array analysis techniques.

3. Source-side scattering

PKIKP precursors can originate from lower mantle scatterers on either the source or receiver side both along and off the great circle ray path (Fig. 1). The source- and receiver-side scattered waves, however, arrived at a seismic station with different incident angle ranges (Fig. 1). Waves generated from the source-side scattering (P to PKPbc or P to PKPab) have larger incident angles (red dotted line in Fig. 1) than those (black dotted lines) from receiver-side scattering (PKPbc to P or PKPab to P). As shown in the Fig. 5 of Cao and Romanowicz (2007), slowness of the receiver-side scattering wave is less than 3.0 s/deg, while those originated from source-side scattering tend to have slowness greater than 3.0 s/deg. We used the beam-forming or slowness-azimuth stacking technique (Aki and Richards, 1980; Niu and Kawakatsu, 1997; Kaneshima and Helffrich, 1998) to measure the slowness and back azimuth of the phase-like precursor shown in Fig. 3a. In a beam-forming analysis, all the seismograms are 2nd-root stacked (Muirhead, 1968) after a time correction calculated from the assumed slowness and back azimuth before stacking. The best slowness and back azimuth were determined when the 2nd-root stacking amplitude reaches to a

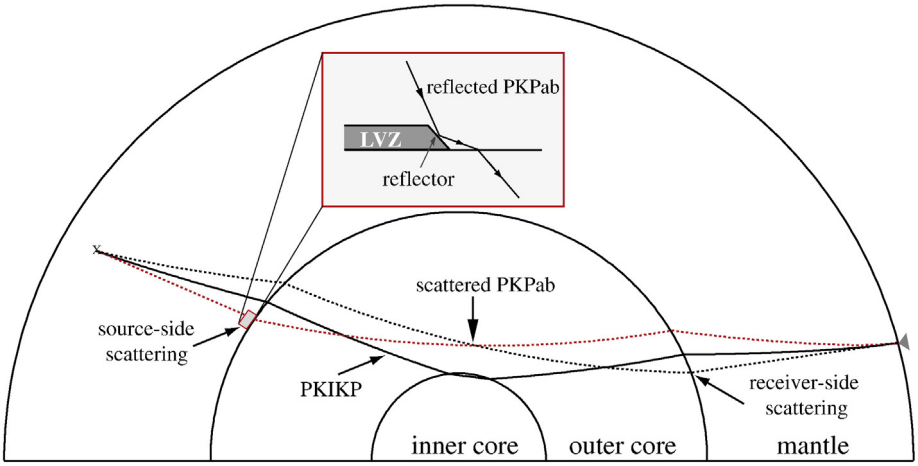

Fig. 1. Schematic diagram of the PKIKP (solid line) and the precursor (red and black dashed lines indicate source and receiver scattering, respectively) phase ray paths used in this study. The gray shaded region is shown in detail within the inset to highlight the reflection rather than scattering geometry. Note that receiver-side scattering (black dotted line) scattering is featured by a larger incident angle in comparison to source-side scattering (red dotted line).

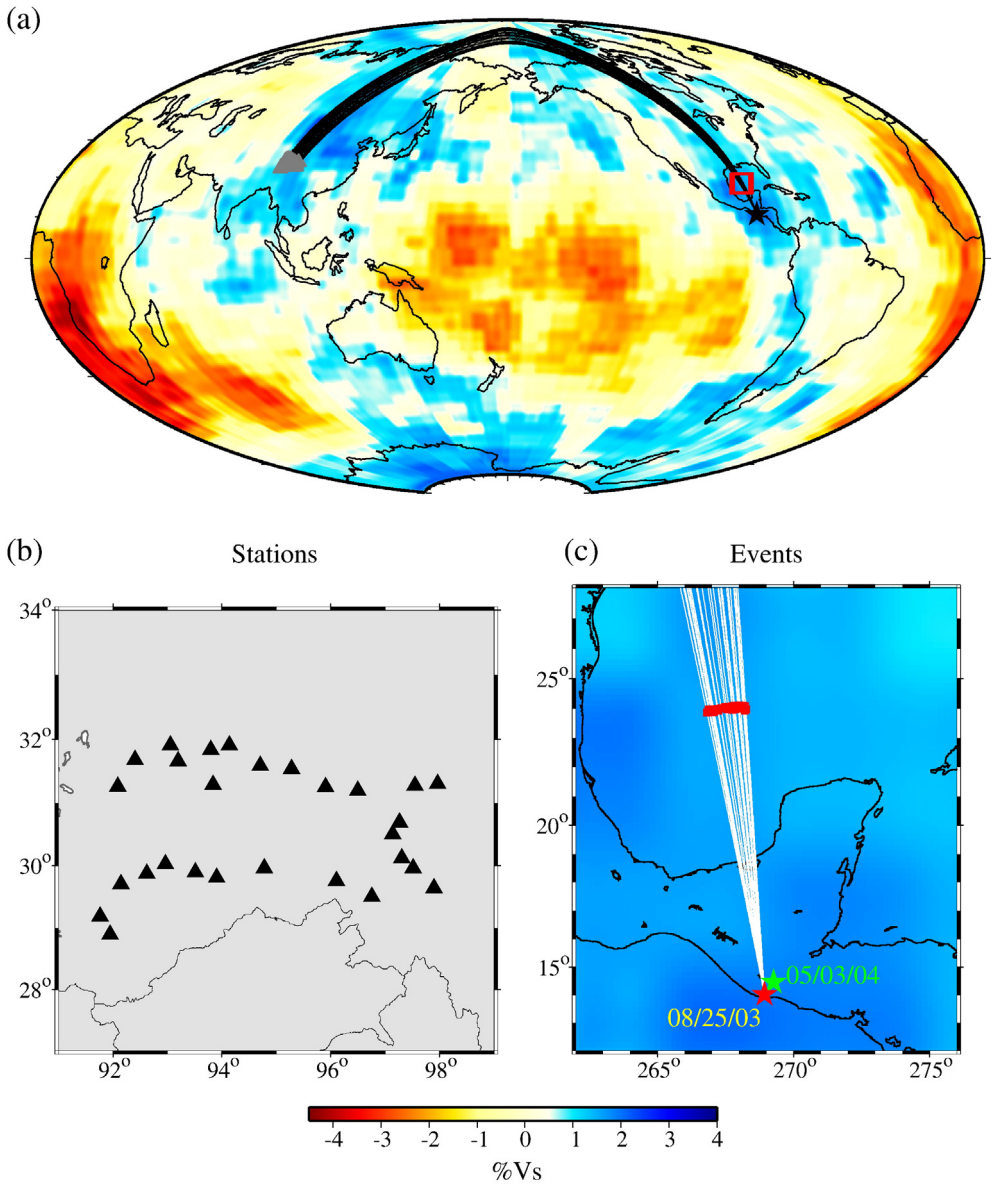

Fig. 2. (a) Event-array geometry with representative PKIKP great circle paths for a source in Central America to the Namche Barwa array in eastern Tibet. (b) Geographic distribution of the station of the Namche Barwa array. (c) The two intermediate depth earthquakes are shown with velocity perturbations in the D″ layer. The region is characterized by a high S-wave velocity anomaly attributed to the ancient subduction of the Farallon plate (Grand, 2002). The 08/25/2003 event (red star) shows a strong, isolated, and well-aligned PKIKP precursor phase. White lines and red squares denote the PKIKP ray paths and their entrance points to the core, respectively. Data from the 05/03/2004 event (green star) did not exhibit any evident PKIKP precursory energy.

maximum (Fig. 4). We varied slowness from 0 to 5 s/deg at increments of 0.05 s/deg, and searched the back azimuth deviation from the great circle path within a range of $\pm 60^{o}$ at increments of 1^{o}. The measured slowness of the precursor is 3.6 ± 0.1 s/deg, much greater than that (1.85 ± 0.1 s/deg) of the PKIKP arrival (Fig. 4). Also the precursor has roughly the same back azimuth as the PKIKP arrival, suggesting that it is due to scattering within the great circle ray path. Such a focused arrival was not found in other precursor time windows as well as the preceding noise windows.

Table 1
Event location and source parameters.

Event date	Event location (lat., lon.)	Event depth (km)	Magnitude (Mw)
08/25/2003	14.03°N, 91.07°W	60.0	5.9
05/03/2004	14.46°N, 91.73°W	124.6	5.7

Although the measured slowness of the precursor arrival is similar to the PKPbdiff waves, we interpreted the short-period precursor observed here as a scattered wave since a diffraction wave has the dominant energy in the low-frequency ($\lesssim$~0.1 Hz) band. We further calculated a series of slownesses and arrival times for D″ scatterers near the entrance and exit points of the PKIKP phase by ray tracing the iasp91 model (Kennett and Engdahl, 1991). We found that for receiver-side scattering a precursory arrival has a slowness less than ~3.1 s/deg. We thus concluded that the observed precursor is due to velocity structure in the source side. Based on the observed slowness, we further interpreted that the precursor is a P to PKPab scattered phase. This is further confirmed from the observed polarity of the PKIKP precursor (Fig. 4c). It is well known that the waveform of PKPab is the Hilbert transform of that of PKIKP. We took the Hilbert transform of the precursor and found that it has a reversed polarity to PKIKP. The reversed polarity seems to be caused by the negative reflection coefficient that will be discussed in the next section.

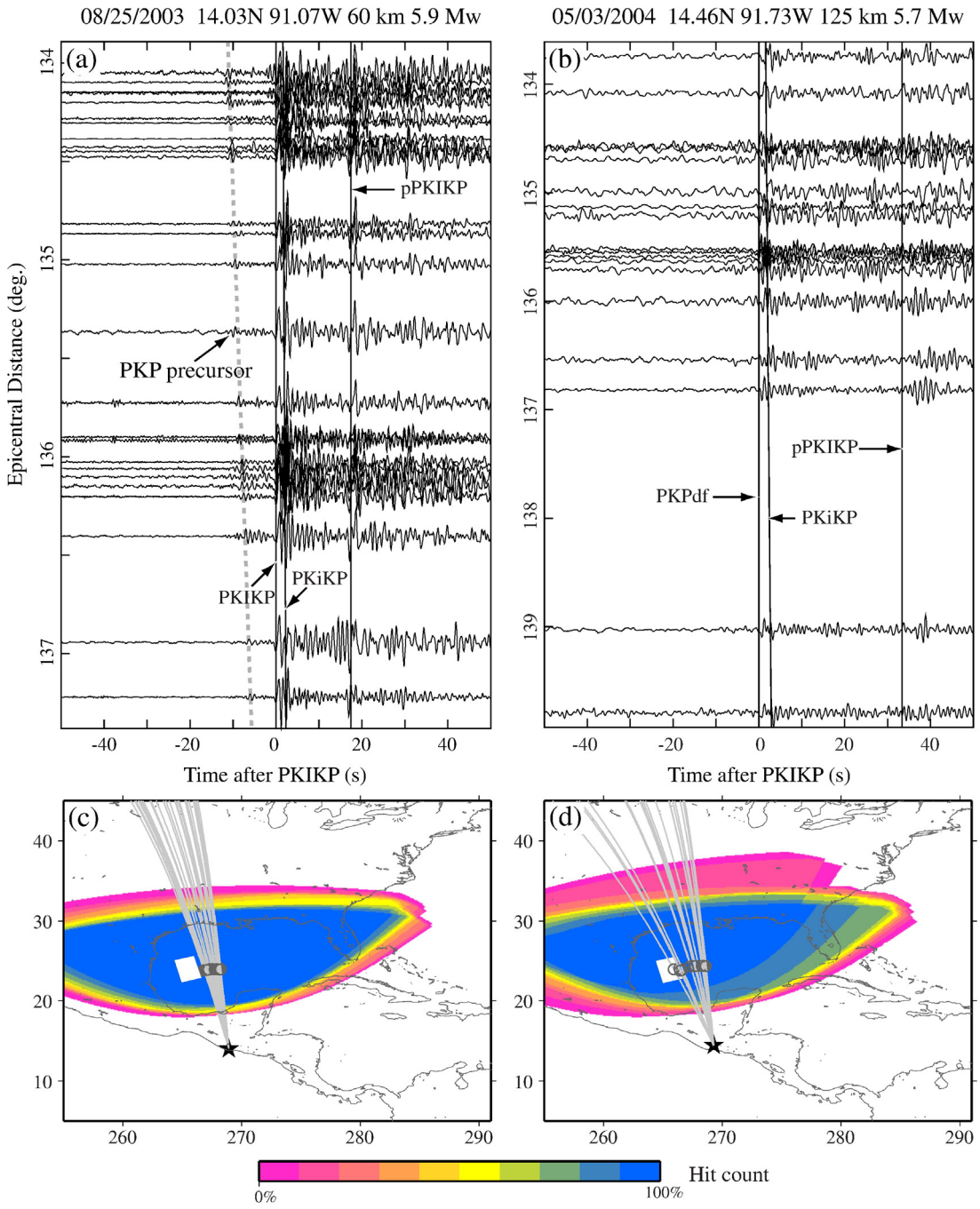

Fig. 3. (a) Selected seismograms for the 08/25/2003 event aligned by the PKIKP arrival time. PKIKP precursor is denoted by the gray dashed line. (b) Selected seismograms for the 05/03/2004 event aligned by the PKIKP arrival time. Note that this event is only ~60 km away from the 2003 event and there are no detectable signals prior to the PKIKP arrival, suggesting that the generation of the precursor is highly dependent upon incident angle. Source regions of precursor scatterers at the CMB in the source side (blue area) are shown together with the identified reflector (white square) for the 2003 (c) and 2004 (d), respectively. Gray lines indicate PKIKP ray paths.

4. Mapping the location and geometry of the seismic scatterers

With the knowledge that the structure responsible for the PKIKP precursor is located along the great circle path in the source side, we employed a migration technique to further characterize the structure. We adopted the method used in Wen (2000) and Niu and Wen (2001) to calculate the probability of scatterer locations beneath the Gulf of Mexico. To examine the overall probable structure in the D″ layer we calculated the probability at two scattering depths, the CMB and 200 km above the CMB. We assumed that PKIKP precursor energy arriving at a certain time is attributed to scatterers along isochronal shells located in the source side. We used iasp91 to compute the isochrones at each assumed scattering depth. To account for 3D effects in the migration moveouts, we manually picked the PKIKP onsets by tracking the relative polarity and moveout of the PKIKP and PKiKP phases. The scatterer probability (Fig. 5a and b) at one grid cell (0.1° by 0.1° cell) is computed from the ratio of the two numbers: number of observations that can be explained by scattering at the grid within a 0.5 second window and the total number of seismic observations used in this study. The hit count at one grid point is simply the total number of PKIKP precursors sampling the grid cell (Fig. 5c and d). Therefore, the grid cells with a large hit count and high probability can be

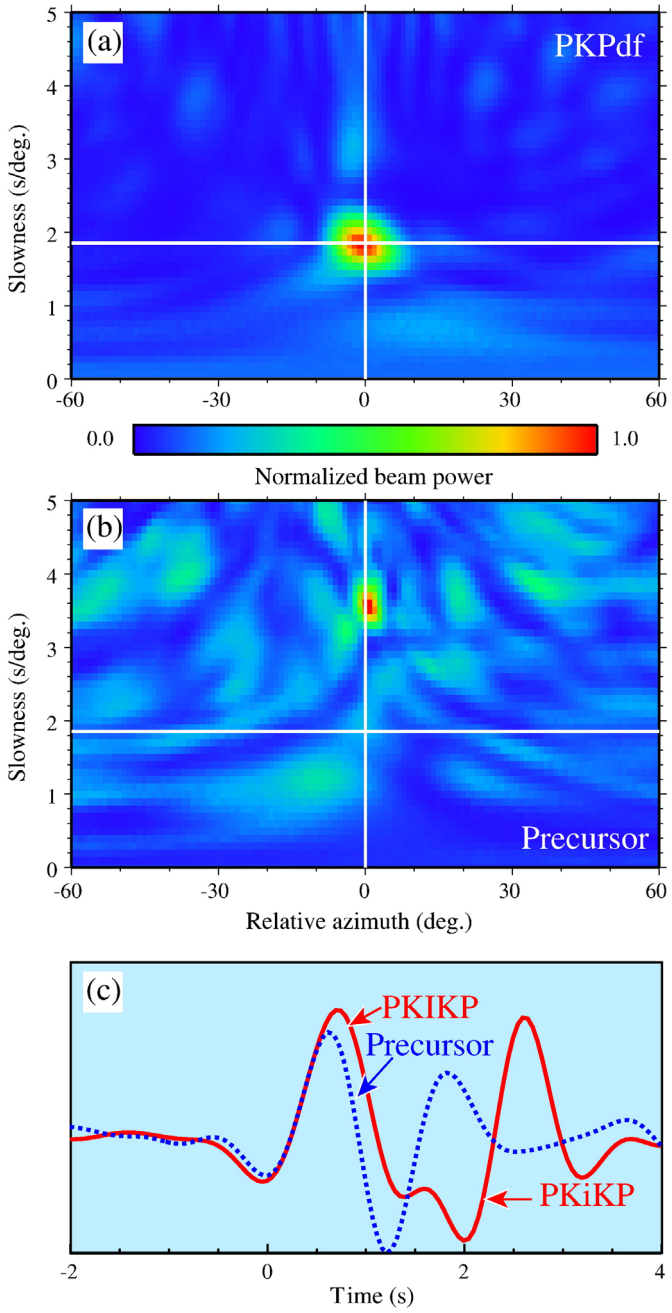

Fig. 4. Normalized energy of the stacked PKIKP (a) and the precursor shown in Fig. 3a (b) is plotted as a function of back azimuth and slowness. A time window of 4 s is used in calculating energy. Note that precursor is received at a larger incident angle (slowness) than the PKIKP, indicating that the reflector is located on the source side. (c) Stacked waveforms of the PKIKP precursor and the PKIKP phase. Note that a Hilbert transform was applied to the precursor waveform and it was further reversed for comparison.

interpreted as the origins of the PKIKP precursor. Areas with large probability can be found at each depth with a peak probability being located slightly to the west of the great circle path (Fig. 5). The slightly westward drift of the peak probability agrees with the back azimuth of the precursor shown in the beam-forming image (Fig. 4b). For example, the back azimuth between the array and the peak location at the CMB (93.8ºW, 25.2ºN) is only 1.5º different from the great circle path between the array and the earthquake. In general, arrival-time picking error is inversely proportional to the SNR of the arrival, which is expected be less than the assumed 0.5 s. This results an uncertainty of $\sim\pm 6$ km in locating the scatterer.

As most of the precursory energy is originated along the great circle path, we further conducted a depth migration to back project the precursor energy to the associated structure. We first calculated the entrance point of PKIKP ray at the CMB from the earthquake to the array center. Within a vertical plane 1º west of the great circle path, we chose a fan area that spans 10º and 200 km in angular and radial directions, respectively. The area centers at the entrance point above the CMB. We divided the area with 0.1º by 5 km grids and search the grids that can best explain the arrival times of the precursor recorded at the array. The computed scatterer probability and the hit count within the area are shown in Fig. 6. We noticed that the scatterer probability increases with depth. The migrated image here indicates that the scatterers form a dipping reflector that generated the observed phase-like precursor. The reflector dips steeply toward the north with a dipping angle of ~52º and is centered at ~93.31ºW and 23.89ºN (Fig. 6).

With the observed orientation of the reflector, we further used 3D ray tracing to calculate the individual reflection points for each source–receiver pair to estimate the lateral extension of the reflector. The reflector is expressed as a plane:

$$h(x,y) = h_0 + h_1(x-x_0)c_1 + h_2(y-y_0)c_2. \quad (1)$$

Here $h(x,y)$ is the height of the reflector above the CMB at a location of (x, y), and h_0 is the height at the reference location (x_0, y_0), which are taken as 100 km, and (93.31ºW, 23.89ºN), respectively. The two horizontal axes x and y are the latitude and longitude (in degree), respectively, and c1 and c2 are two constants of unit conversion from degree to kilometer in the two directions at the core–mantle boundary. Starting from a point in the reflector, we first use one-dimensional ray tracing to find the two ray paths that join the start point to the source and receiver, respectively. We represent the incident and reflected directions as two three-dimensional unit vectors $\mathbf{n_1}$ and $\mathbf{n_2}$. Based on Snell's law, the normal vector of the reflector of the P-to-P reflection, $\mathbf{n}$, is

$$\mathbf{n} = \mathbf{n}_1 + \mathbf{n}_2. \quad (2)$$

We then search for the point at the reflector whose $\mathbf{n}$ calculated from (2) coincides with the normal vector of the reflector plane represented by Eq. (1). The calculated reflection points show that the reflector extends at least 100 km in the east–west direction.

5. Discussion

We have imaged a steeply dipping reflector at the base mantle beneath the Gulf of Mexico from a phase-like PKIKP precursor; this observation is clearly different from the generally accepted notion that these precursors solely represent volumetric scattering or CMB topography (Haddon, 1972; Cleary and Haddon, 1972; Hedlin et al., 1997; Shearer et al., 1998). Thus we are left with the challenge to develop a plausible interpretation of the structure in a region that is dominated by the ancient Farallon slab remnants at the base of the mantle (Kendall and Nangini, 1996; Grand, 2002). The average amplitude ratio between the precursor and PKIKP is approximately 0.2. With an incident angle of ~78º, a velocity contrast of a few to 10% is required to account for the observed amplitude of the precursor. As the P to P reflection coefficient depends also on S-wave velocity contrast, the constraint on the P-wave velocity contrast is rather weak. To determine whether the velocity increases or decreases with depth, we compared the polarity between the precursor and the PKIKP waveforms. A Hilbert transform was first applied to the waveforms of the precursor before the comparison, as the precursor is a P to PKPab reflected wave. The two phases have opposite polarity, suggesting that P-wave velocity drops from the upper to the lower side of the boundary (Fig. 4c).

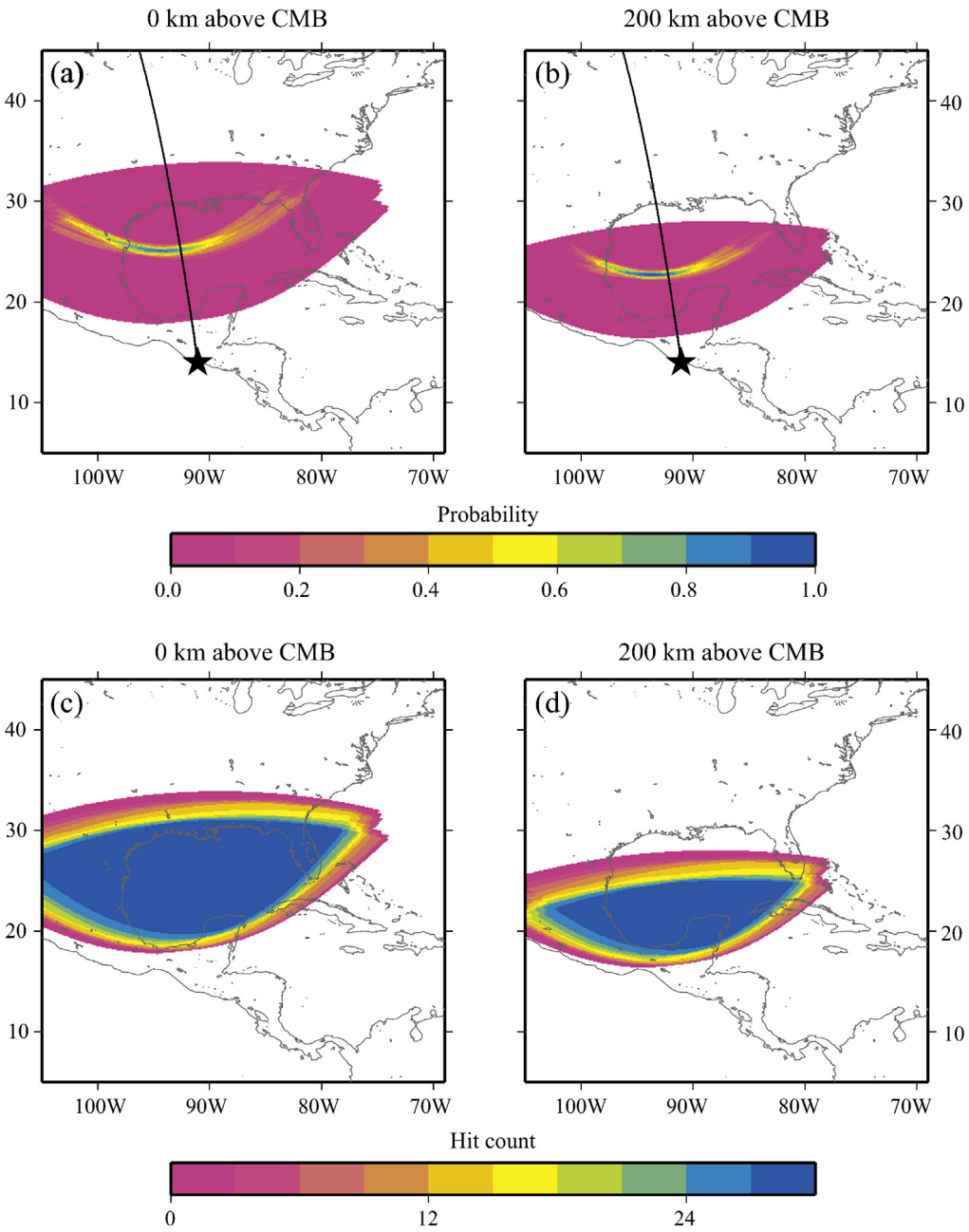

Fig. 5. Maps of the "scatterer probability" at depths: 0 km (a) and 200 km (b) above the CMB. Note the blue arcs in a and b, which defines the seismic reflector that produced the observed the precursor. Hit count at the two depths are shown in c and d, respectively.

Recent seismological studies and advancements in mineral physics, namely the discovery and characterization of the post-perovskite phase, have led to new interpretations of both the D″ discontinuity as well as some low velocity layers observed at the base of the mantle (Murakami et al., 2004; Lay et al., 2006; Wookey et al., 2005; Wentzcovitch et al., 2006; Hernlund et al., 2005). In a cold environment, the ppv phase is thought to have a double crossing of the phase boundary forming ppv lenses in the D″ layer. Both the post-perovskite phase transition and its reverse can result in seismic discontinuities in the lowermost mantle (Hernlund et al., 2005; van der Hilst et al., 2007). This double-crossing model, however, cannot explain the large velocity drop and the steeply dipping geometry of the observed reflector.

It also should be noted that the observed PKIKP precursor is unlikely to be generated by the CMB topography. Geodynamic modeling and seismological observations have constrained the amplitude of CMB topography to be less than 10 km with an average between 3 and 6 km (Creager and Jordan, 1986; Morelli and Dziewonski, 1987; Doornbos and Hilton, 1989). Consequently, if the CMB topography is the main source for generating the observed precursor, then most of the precursory energy is expected to be in high frequency ($\geq$2 Hz), as the wavelength of the scattering wave should be comparable to the size of the characteristic length of the CMB topography. Beneath the Gulf of Mexico CMB topography is observed to be $\pm$3 km, Sze and van der Hilst (2003) observed a CMB topography of less than $\pm$3 km beneath the Gulf of Mexico, pushing the frequency further to the high end. The observed precursor is still discernable in the frequency lower than 1 Hz, making such topography an unlikely interpretation of the feature observed in this study. Also a P-to-PKPab arrival reflected at a dipping CMB is expected to be much larger (0.3) than the observed precursor amplitude (~0.2 of the PKIKP).

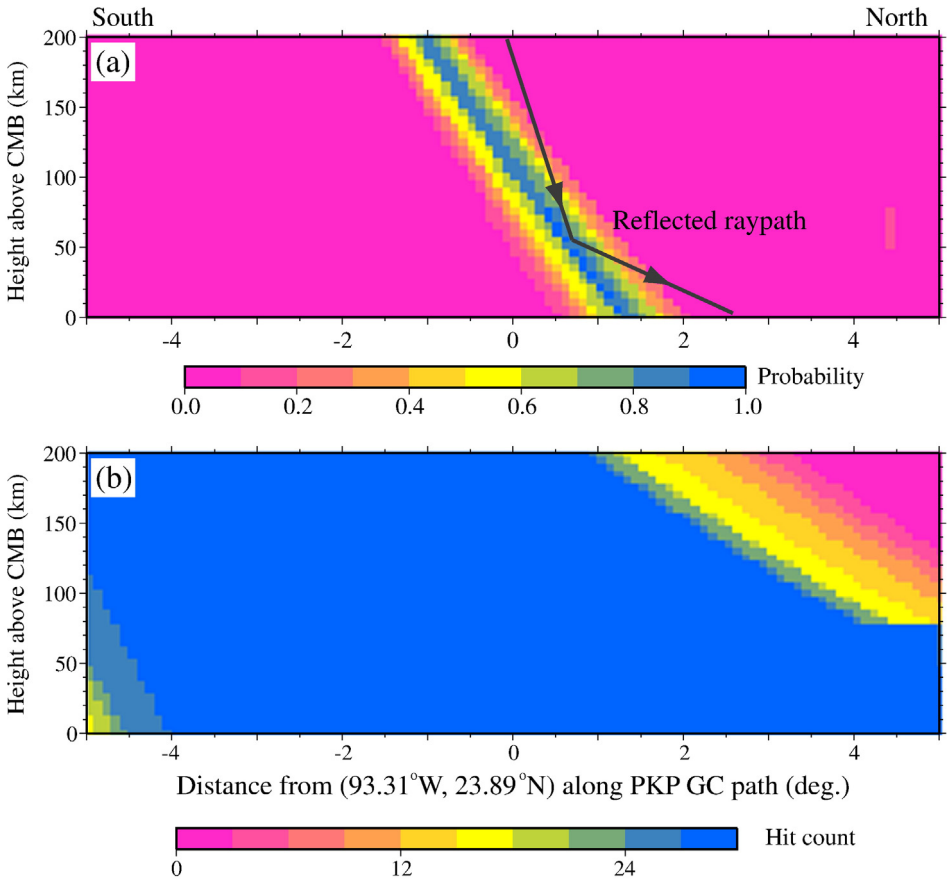

Fig. 6. (a) Cross sectional view of the migration results centered about 93.31ºW and 23.89ºN and in a nearly South–North direction from left to right. The migrated image indicates that the observed reflector dips northward at ~52º and becomes more significant in the lowermost ~100 km of the mantle. (b) Hit count for the ray paths in the cross-section.

Since velocity decreases across the boundary, it is natural to consider the region below the reflector is an ULVZ or a low velocity zone (LVZ) depending the magnitude of velocity reduction in this region. Havens and Revenaugh (2001) found a laterally varying and intermittent ULVZ in our study region, but its presence was not confirmed by a more recent study (Hutko et al., 2009). The thickness of the ULVZ/LVZ is not well constrained. It is likely that the ULVZ/LVZ is confined within the a few tens of kilometers right above the CMB, as the computed scatterer probability increases with depth. The northward dipping reflector is this simply the northern edge of the ULVZ/LVZ. Previous studies probed the region beneath the Gulf of Mexico, Central America, and west of Mexico to search for ULVZs, but found mixed and even contradictory results (see Thorne and Garnero, 2004 for a review; Persch et al., 2001; Castle and van der Hilst, 2000; Niu and Wen, 2001). Additionally, there are evidences for strong lateral heterogeneity beneath the Caribbean. Especially, a high-attenuation and low velocity structure was identified at the base of the mantle and was interpreted as a possible region of trapped mantle material beneath the Farallon slab (Wysession et al., 2001; Tkalčić and Romanowicz, 2002; Fisher et al., 2003). Our observation is consistent with these observations that there is a large amount of small-scale heterogeneity present beneath the subducted Farallon slab. We are therefore left with the question on how a low velocity lens can be developed beneath the remnant Farallon slab.

ULVZs are commonly observed in association with the edges of large thermochemical structures (e.g. Thorne and Garnero, 2004; Garnero and McNamara, 2008 for review). Moreover, steeply dipping reflectors with a scale similar to the one observed in this study have been detected in connection with the large-scale low velocity anomaly beneath Africa (Wen, 2000). These seismic observations are consistent with recent geodynamic modeling of thermochemical piles, which suggests that ULVZs tend to form along the edge of these large low velocity structures (Tan and Gurnis, 2005). However, the cold environment in this study requires a different mechanism to generate the observed ULVZ/LVZ.

One possible mechanism to generate an ULVZ in a cold environment invokes long-term heating of the base of a subducted slab lying above the CMB. Tan et al. (2002) found that subducted slabs can have important consequences on plume formation. While plumes tend to preferentially develop on the edge of slabs, a “mega-plume” can be developed beneath the subducted slabs as a consequence of long-term

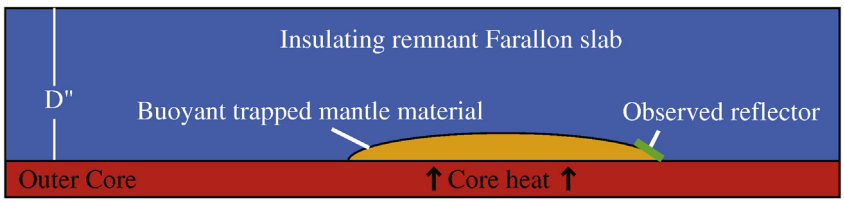

Fig. 7. A schematic diagram showing our preferred interpretation of the ULVZ/LVZ, which is developed underneath a subducted slab due to continuous heating from the core. The edge of the ULVZ/LVZ acts as a seismic reflector that generates the precursory energy.

heating from core. Thus, the lower velocity structure observed here could reflect a thin hot layer sandwiched by the cold slab and hot core. The ULVZ/LVZ could be developed from the lower part of the subducted oceanic lithosphere or trapped mantle material. Hereafter we make no difference between them and refer them as to trapped mantle material. The trapped mantle material becomes geodynamically unstable with a thermal buoyant force. Over time, the instability would develop into a patch of low velocity that has steeply dipping edges acting as effective seismic reflectors (Fig. 7). This model is also consistent with measurements of anisotropy in the lowermost mantle beneath the Gulf of Mexico. Garnero et al. (2004) found a highly variable azimuthal anisotropy with lateral variations on the order of ~100 km in the region.

An alternative model requires the entrapment of iron-rich ppv beneath the Farallon slab corresponding to the low velocity structure (Mao et al., 2006). This iron-enriched material is expected to be significantly denser than the surrounding mantle such that it tends to collapse into a flat thin layer (less than a few kilometers) at the base of mantle depending on the viscosity difference with the surrounding mantle (Mao et al., 2006). Maintaining a relatively thick layer with seismically visible edge thus requires external forces. The region beneath the Gulf of Mexico is not known to have been a source of large-scale upwelling in recent geologic history and is dominated by the history of the Farallon subduction between 100 and 46 Ma (Pindell et al., 2005). In order to invoke this mechanism, one needs significant involvement from the subducting slab or other unknown processes to maintain a dense iron-rich ppv pile. Because of this, we prefer the trapped mantle model discussed in the last paragraph as the likely interpretation of the observed reflector and the ULVZ/LVZ.

6. Conclusions

We observed a clear phase-like PKIKP precursor at a broadband array in eastern Tibet from one intermediate depth earthquake in Central America. This precursor was not shown in the seismograms recorded by the same array from another earthquake only ~60 km away. We interpreted this difference by a reflection geometry, which depends highly on the illumination direction from a source. The reflection requires a steeply dipping boundary that centers at ~93.31ºW and 23.89ºN right above the CMB beneath the Gulf of Mexico. P-wave velocity drops by a few to 10% across this boundary. Because of its dipping geometry and the large velocity drop, it is unlikely that this boundary is caused by the post-perovskite phase transition or the reverse transformation. We interpreted this boundary as the edge of a ULVZ/LVZ and further speculated that the ULVZ/LVZ was developed beneath the subducted Farallon slab as a consequence of long-term heating from core.

Acknowledgments

We thank the IRIS data for providing the waveform data. We also thank the field team of the “Geodynamics of Indentor Corners” project led by the Lehigh University for collecting the high quality data. Discussions with X. Cheng and M. Miller were helpful in preparing the manuscript. Critical comments from two anonymous reviewers significantly improved the quality of this paper. This work was supported by the NSF grant EAR-0748455. Y. Ma was also supported by the NSFC grant 40574024.

References

Aki, K., Richards, P.G., 1980. Quantitative Seismology. Freeman and Co., New York.
Cao, A., Romanowicz, B., 2007. Locating scatterers in the mantle using array analysis of PKP precursors from an earthquake doublet. Earth and Planet. Sci. Lett. 255, 22–31.
Castle, J.C., van der Hilst, R.D., 2000. The core–mantle boundary under the Gulf of Alaska: no ULVZ for shear waves. Earth and Planet. Sci. Lett. 176, 311–321.
Cleary, J.R., Haddon, R.A.W., 1972. Seismic wave scattering near the core–mantle boundary: a new interpretation of precursors to PKP. Nature 240, 549–551.
Creager, K., Jordan, T., 1986. Large-scale structure of the outermost core from P′df and P′ ab travel times, in EOS, Trans. AGU 67, 311.
Doornbos, D.J., Hilton, T., 1989. Models of the core–mantle boundary and the travel times of internally reflected core phases. J. Geophys. Res. 94, 15 741–15 751.
Doornbos, D.J., Husebye, E.S., 1972. Array analysis of PKP phases and their precursors. Phys. Earth Planet. Inter. 5, 387–399.
Fisher, J.L., Wysession, M.E., Fischer, K.M., 2003. Small-scale lateral variations in D″ attenuation and velocity structure. Geophys. Res. Lett. 30, 1435. doi:10.1029/2002GL016179.
Garnero, E.J., 2004. A new paradigm for Earth's core–mantle boundary. Science 304. doi:10.1126/science.1097849.
Garnero, E.J., McNamara, A.K., 2008. Structure and dynamics of Earth's lower mantle. Science 320, 626–628.
Garnero, E.J., Grand, S.P., Helmberger, D.V., 1993. Low P-wave velocity at the base of the mantle. Geophys. Res. Lett. 20, 1843–1846.
Garnero, E.J., Maupin, V., Lay, T., Fouch, M.J., 2004. Variable azimuthal anisotropy in Earth's lowermost mantle. Science 306, 259–261.
Grand, S.P., 2002. Mantle shear-wave tomography and the fate of subducted slabs. Phil. Trans. R. Soc. Lond. 360, 2475–2491.
Haddon, R.A.W., 1972. Corrugations on the CMB or transition layers between inner and outer cores? Eos 53, 600.
Haddon, R.A., Cleary, J.R., 1974. Evidence for scattering of seismic PKP waves near the core–mantle boundary. Phys. Earth Planet. Inter. 8, 211–234.
Havens, E., Revenaugh, J., 2001. A broadband seismic study of the lowermost mantle beneath Mexico: constraints on ultralow velocity zone elasticity and density. J. Geophys. Res. 106, 30 809–30 920.
Hedlin, M.A.H., Shearer, P., 2000. An analysis of large-scale variations in small-scale heterogeneity throughout the earth's mantle. J. Geophys. Res. 105, 13 655–13 673.
Hedlin, M.A.H., Shearer, P.M., Earle, P.S., 1997. Seismic evidence for small-scale heterogeneity throughout Earth's mantle. Nature 387, 145–150.
Helffrich, G., Wood, B., 2001. The Earth's mantle. Nature 412, 501–507.
Hernlund, J., Thomas, C., Tackley, P.J., 2005. A doubling of the post-perovskite phase boundary and structure of the Earth's lowermost mantle. Nature 434, 882–886.
Hutko, A.R., Lay, T., Revenaugh, J., 2009. Localized double-array stacking analysis of PcP: D″ and ULVZ structure beneath the Cocos plate, Mexico, central Pacific, and north Pacific. J. Phys. Earth Planet. Inter. 173, 60–74.
Kaneshima, S., Helffrich, G., 1998. Detection of lower mantle scatterers northeast of the Mariana subduction zone using short-period array data. J. Geophys. Res. 103, 4825–4838.
Kendall, J.M., Nangini, C., 1996. Lateral variations in D″ below the Caribbean. Geophys. Res. Lett. 23, 399–402.
Kennett, B.L.N., Engdahl, E.R., 1991. Travel times for global earthquake location and phase identification. Geophys. J. Int. 105, 429–465.
Lay, T., Garnero, E.J., 2004. Core–Mantle Boundary Structures and Processes. In: Sparks, R.S.J., Hawkesworth, C.J. (Eds.), The State of the Planet: Frontiers and Challenges in Geophysics: Geophysical Monograph 150, IUGG, Volume 19. doi:10.1029/150GM04.
Lay, T., Hernlund, J., Garnero, E.J., Thorne, M.S., 2006. A post-perovskite lens and D″ heat flux beneath the Central Pacific. Science 314, 1272–1276.
Mao, W.L., Mao, H., Sturhahn, W., Zhao, J., Prakapenka, V.B., Meng, Y., Shu, J., Fei, Y., Hemley, R.J., 2006. Iron-rich post-perovskite and the origin of ultralow-velocity zones. Science 312, 564–565.
Meltzer, A., Sol, S., Zurek, B., Xuanyang, Z., Jianlong, Z., Wenqing, T., 2003. The Eastern Syntaxis Seismic Experiment. EOS Trans. Am. Geophys. Union 84 (46), T42B–T0292B.
Miller, M., Niu, F., 2008. Bulldozing the core–mantle boundary: localized seismic scatterers beneath the Caribbean Sea. PEPI 170, 89–94.
Morelli, A., Dziewonski, A.M., 1987. Topography of the core–mantle boundary and lateral homogeneity of the liquid core. Nature 325, 678–683.
Muirhead, K.J., 1968. Eliminating false alarms when detecting seismic events automatically. Nature 217, 533–534.
Murakami, M., Hirose, K., Kawamura, K., Sata, N., Ohishi, Y., 2004. Post-perovskite phase transition in MgSiO3. Science 304, 855–858.
Niu, F., Kawakatsu, H., 1997. Depth variation of the mid-mantle seismic discontinuity. Geophys. Res. Lett. 24, 429–432.
Niu, F., Wen, L., 2001. Strong seismic scatterers near the core–mantle boundary west of Mexico. Geophys. Res. Lett. 28, 3557–3560.
Persch, S., Vidale, J.E., Earle, P.S., 2001. Absence of a short-period ULVZ precursors to PcP and ScP from two regions of the CMB. Geophys. Res. Lett. 28, 387–390.
Pindell, J., Kennan, L., Maresch, W.V., Stanek, K.-P., Draper, G., Higgs, R., 2005. Plate-Kinematics and Crustal Dynamics of Circum–Caribbean Arc–Continent Interactions: Tectonic Controls on Basin Development in Proto-Caribbean Margins. In: Lallemant, H.G., Sisson, V.B. (Eds.), Caribbean–South American Plate Interactions. Venezuela. Geological Society of America, Boulder, CO, pp. 7–52.
Rost, S., Garnero, E.J., Williams, Q., Manga, M., 2005. Seismological constraints on a possible plume root at the core–mantle boundary. Nature 435, 666–669.
Shearer, P.M., Hedlin, M.A.H., Earle, P.S., 1998. PKP and PKKP Precursor Observations: Implications for the Small-scale Structure of the Deep Mantle and Core. In: Region, The Core–Mantle Boundary (Ed.), Geodynamics, 28. American Geophysical Union, Washington, DC, pp. 37–55.
Sze, E.K.M., van der Hilst, R.D., 2003. Core mantle boundary topography from short period PcP, PKP and PKKP data. Phys. Earth planet. Inter. 135, 27–46.
Tan, E., Gurnis, M., 2005. Metastable superplumes and mantle compressibility. Geophys. Res. Lett. 32, L20307. doi:10.1029/2005GL024190.
Tan, E., Gurnis, M., Han, L., 2002. Slabs in the lower mantle and their modulation of plume formation. Geochem. Geophys. Geosyst. 3, 1067. doi:10.1029/2001GC000238.
Thomas, C., Weber, M., Wicks, C.W., Scherbaum, F., 1999. Small scatterers in the lower mantle observed at German broadband arrays. J. Geophys. Res. 104, 15073–15088.
Thorne, M.S., Garnero, E.J., 2004. Inferences on ultralow-velocity zone structure from a global analysis of SPdKS waves. J. Geophys. Res. 109, B08301. doi:10.1029/2004JB003010.

Tkalčić, H., Romanowicz, B., 2002. Short scale heterogeneity in the lowermost mantle: insights from PcP-P and ScS-S data. Earth Planet. Sci. Lett. 201, 57–68.
van der Hilst, R.D., De Hoop.,, M.V., Wang, P., Shim, S.-H., Tenorio, L., Ma, P., 2007. Seismostratigraphy and thermal structure of Earth's core–mantle boundary region. Science 315, 1813–1817.
Vidale, J.E., Hedlin, M.A.H., 1998. Evidence for partial melt at the core–mantle boundary north of Tonga from the strong scattering of seismic waves. Nature 391, 682–685.
Wen, L., 2000. Intense seismic scattering near the core–mantle boundary beneath the Comoros hotspot. Geophys. Res. Lett. 27, 3627–3630.
Wen, L., Helmberger, D.V., 1998. Ultra-low velocity zones near the core–mantle boundary from broadband PKP precursors. Science 279, 1701–1703.
Wentzcovitch, R.M., Tsuchiya, T., Tsuchiya, J., 2006. MgSiO3 post perovskite at D″ conditions. Proc. Natl. Acad. Sc. 103, 543–546.
Williams, Q., Garnero, E.J., 1996. Seismic evidence for partial melt at the base of Earth's mantle. Science 273, 1528–1530.
Wookey, J., Stackhouse, S., Kendall, J.-M., Brodholt, J., Price, G.D., 2005. Efficacy of the post-perovskite phase as an explanation for lowermost-mantle seismic properties. Nature 438, 1004–1007.
Wysession, M.E., Fischer, K.M., Al-eqabi, G.I., Shore, P.J., Gurari, I., 2001. Using MOMA broadband array ScS-S data to image smaller-scale structures at the base of the mantle. Geophys. Res. Lett. 28, 867–870.